# Transference of potentially toxic elements from soils to plants in a derelict Pb-Zn mining area (San Quintín mine, South-Central Spain)

**José Ignacio Barquero Peralbo**

joseignacio.barquero@uclm.es

University of Castilla-La Mancha: Universidad de Castilla-La Mancha https://orcid.org/0000-0002-7716-3356

**Jesús Peco**

**Jaime Villena**

**Juan Antonio Campos**

**José María Esbrí**

**Francisco J. García-Navarro**

**Marta María Moreno**

**Pablo Higueras**

**Research Article**

**Keywords:** Potentially toxic elements (PTEs), Soil–plant transfer, Bioaccumulation, Abandoned mining areas, San Quintín mine

**Posted Date:** July 7th, 2025

**DOI:** https://doi.org/10.21203/rs.3.rs-6991303/v1

# Abstract

Background and aims: Abandoned mining areas represent critical environmental pollution hotspots due to the persistence of waste materials enriched in potentially toxic elements (PTEs). This study evaluates the transfer of PTEs from contaminated soils to six plant species in the vicinity of the San Quintín Pb-Zn mine (Ciudad Real, Spain), a site impacted by over a century of mining activity.

Methods: The studied species include the tree *Quercus ilex*, the shrubs *Retama sphaerocarpa* and *Scrophularia canina*, and the annual herbaceous species *Spergularia rubra*, *Rumex bucephalophorus*, and *Hirschfeldia incana*. Soil and plant tissue samples were analysed using X-ray fluorescence and atomic absorption spectrometry to determine concentrations of Zn, Pb, Hg, Cu, and other PTEs.

Results: Results revealed a high heterogeneity in the bioaccumulation of elements such as Zn, Pb, Hg, and Cu among the studied species, with *Spergularia rubra* and *Rumex bucephalophorus* emerging as effective bioindicators of soil contamination. Specific correlations between soil and plant concentrations were identified, and atmospheric uptake was found to significantly influence Hg accumulation in plant tissues.

Conclusions: This work enhances our understanding of plant uptake mechanisms in contaminated environments and provides a foundation for ecological restoration and environmental monitoring strategies in decommissioned mining areas, emphasizing the role of both edaphic properties and species-specific physiological adaptations.


# INTRODUCTION

Plants absorb essential elements, including Cu, Ni, Fe, Zn, Mn, and Mo, which are required for their normal physiological functions. However, when their concentrations exceed certain thresholds, these essential elements can also induce phytotoxic effects. In addition to these, plants can absorb non-essential elements with no known biological function, some of which are highly toxic (Kirkby, 2012; Peco et al., 2021). Both essential elements that become toxic at elevated concentrations and inherently toxic non-essential elements are collectively referred to as potentially toxic elements (PTEs) (Kisku et al., 2000; Thalassinos et al., 2023). Different plant species employ distinct mechanisms for the uptake of these elements from the soil. Nevertheless, the efficacy of this uptake strongly depends on the bioavailability of these elements in the soil (Newman et al., 1994). The so-called bioavailability, constrained by the chemical state or speciation of the elements, is conditioned by different factors (Galán & Romero, 2008). Primary among these factors are climate conditions, which control water availability and its temperature-dependent activity in the soil. Additionally, geochemical behaviour, mineralogical form, and the presence of biological populations in the soil, capable of reacting with minerals containing the elements and potentially destroying their crystalline structure, are noteworthy contributors (Molina et al., 2006; Kabata Pendias, 2011). As a result, the absorption of PTEs in plants is a highly intricate process due to the multitude variables involved. Going even further, the uptake of PTEs from the soils can favour their bioaccumulation in edible parts, producing a risk for the incorporation of PTEs (especially in toxic concentrations) into vertebrates, including humans. This situation becomes a significant public health concern (Kabata Pendias, 2011; Adamo et al., 2014).

Decommissioned mining areas are of particular interest for the study of the process of elemental incorporation into plants and assessing risks related to such process. Mining areas, especially those abandoned before the development of an ecological consciousness, act as sources of PTEs for nearby agronomic fields. This is due to the eventual persistence of waste accumulations that can be easily disseminated with the help of rainwater and wind to the neighbour areas (Sánchez-Donoso et al., 2019). The presence of pyrite ($FeS_2$) in the mined ores is of particularly concern, since this mineral is easily hydrolysed in atmospheric conditions, producing acidity which also favours the hydrolysis of the rest of metallic sulphides, in particular sphalerite (ZnS), galena (PbS) and chalcopyrite ($CuFeS_2$) (Harries and Ritchie, 1987). This process induces the release of corresponding PTE ions into the soils, taking on different solubility forms depending on the geochemical affinity of each ion for others. For instance, $Pb^{2+}$ readily combine with $SO_4^{2+}$ or $CO_3^{2+}$, giving origin to insoluble anglesite ($PbSO_4$) or cerussite ($PbCO_3$).

The San Quintín Pb-Zn-Ag area, located in the Southern Central Iberian Zona of the Hesperian Massif, exploited a mineralization hosted by shales and greywackes of pre-Ordovician age, and constituted by a typically hydrothermal mineral paragenesis comprising all the previously mentioned minerals: galena rich in silver (most probably due to the presence of Ag sulfosalts associated to it), sphalerite, chalcopyrite (scarce), and abundant pyrite, with quartz and minor calcite as ganga minerals (Palero, 1991). Also, after this author, the mine was active since old times, with a most important period of activity between years 1894 and 1923, and with a declared production of galena concentrates of some 500 000 tonnes. As a result of this activity, piles of residua with high residual concentration of Zn were left in the area, due to the low price of this element. But in the 1950's, the increase in the price of this element, used in galvanization in the automotive industry, supposed the installation in the area of a 'modern' froth flotation plant, in which the former residua were in part reprocessed to obtain Zn, Pb and Ag. This plant produced two types of tailings: the materials with lower grain size, including silt and clay, were disposed in an embarquement dam, meanwhile the materials with sand size passed though the froth flotation process and the residua were accumulated in a tailings pile. In 1990 an experimental test to obtain cinnabar (HgS) concentrates from the ore coming from the Almadén mercury mine (located some 80 km to the West; Hernández et al., 1999, among many others) was performed, and both residua on the original ore and of the cinnabar concentrates obtained were also abandoned in the area. After that, in the same year 1990 the froth flotation plant was abandoned, as well as the still unprocessed dumps and the dams. It is worth to note that an old gallery for dumps drainage produce seasonal outputs of Acid Mine Drainage (AMD) (Fig. 1B), with very low pH (2 in average) and with high saline concentration (Electric conductivity > 8000 μS-cm$^{-1}$ as a norm). The area is at present under remediation, funded by European Next Generation funds.

Previous studies in the area have characterized elemental contents in soils and their speciation (Rodríguez et al., 2009). Other investigations have compared the composition of the tailings with those from other exploited ore deposits in the region (Higueras et al., 2011); assessed the transference of PTEs from soil to acorn-tree (*Quercus ilex*) leaves, transference of PTEs also on a regional basis (Higueras et al., 2017); studied the geomorphology of the wastes piles to obtain conclusions on the dispersion processes of the fine material by water and wind (Sánchez-Donoso et al., 2019; 2021); assessed the toxicity of the waste materials using integrated geochemical and toxicological studies (García-Lorenzo et al., 2019; Ferri-Moreno et al., 2023); and studied the microbial diversity of the different types of soils present in the area (Gallego et al., 2021) and its influence of the mobility of PTEs in the soil (Peco et al., 2023). These studies conclude that the area is heavily contaminated, with soils containing potentially toxic elements (PTEs) within the ranges reported by Rodríguez et al. (2009) and Higueras et al. (2011). Notably, elevated concentrations of Pb, Zn, Hg, and Cd have been detected in *Quercus ilex* leaves (Higueras et al., 2017), and the presence of mine residues poses a significant risk to living organisms (García-Lorenzo et al., 2019; Ferri-Moreno et al., 2023). Additionally, different types of soils exhibit distinct microbial population, each influencing the mobility and bioavailability of PTEs (Gallego et al., 2021; Peco et al., 2023).

In the present study, we have used the San Quintín area as a natural laboratory, providing a unique opportunity to investigate the long-term impact of waste (most for over 100 years) on the environment. The study focuses on plant-soil interactions, particularly with plants living in the area since time before the main mine activity occurred (*Q. Ilex*), as well growing directly on the waste material, including long-standing species like *Retama sphaerocarpa* and *Scrophularia canina*, as well as annual species like *Spergularia rubra*, *Rumex bucephalophorus* and *Hirschfeldia incana*. Besides, we have a high number of previous studies based in the soil properties, very useful to complete the portrait of the area. The comprehensive analysis, including plants assessments presented in this study, contributes to evaluating the intricate plant-to-soil transfer process in this complex environment. This investigation serves as a basis to understand the peculiarities of processes in extreme environments, specifically decommissioned mine areas affected by AMD, and in an evolved state of vegetal cover regeneration.

The main objectives of this study have been: a) to perform a detailed geochemical characterization of the San Quintín mining area, focusing on the distribution, speciation, and mobility of potentially toxic elements (PTEs) in soils and mining residues; b) to assess the species-specific patterns of PTE uptake and bioaccumulation in native and colonizing plants, identifying key physiological and environmental factors influencing this process and evaluating their potential as bioindicators or candidates for phytoremediation in contaminated environments; and c) to investigate the role of atmospheric deposition in mercury accumulation in plant tissues, considering species morphology and proximity to emission sources.

The insights gained are not only valuable for assessing risks withing this environment concerning the human food chain but also hold significance for similar areas affected by similar contamination processes.

# MATERIALS AND METHODS

Sampling and processing

*Site description and sampling*

Soil sampling was conducted in the eastern sector of the San Quintín area, selected for its broader spatial extent, high plant species diversity, and the presence of distinct environmental domains warranting detailed characterization. A total of 23 sampling sites were established, distributed across three primary domains: the area containing the oldest mining residues (5 sites), zones affected by the froth flotation process (7 sites), and peripheral soils (11 sites) (Fig. 1). According to data reported by Rodríguez et al. (2009), the highest concentrations of PTEs were found in the oldest wastes deposits, followed by the flotation tailings. Peripheral soils exhibited substantial variability in PTE concentrations, likely influenced by their proximity to contaminated zones, as well as by secondary dispersion mechanisms such as wind erosion, surface runoff, and post-mining anthropogenic activities.

At each selected site, chosen based on the presence of vegetation of particular ecological or conservation interest, a composite soil sample was collected by excavating up to a maximum depth of 20 cm. In certain locations, this depth could not be reached due to excessive soil compaction, likely resulting from historical anthropogenic disturbances such as former waste deposits. Three subsamples were extracted from randomly distributed points within a 10–15 $m^2$ plot to ensure spatial representativeness. Approximately 5 kg of soil per site was obtained, homogenized, and stored in high-density polyethylene (HDPE) bags, properly labelled with site code, date, and sample ID. All samples were transported under ambient conditions and stored at 4°C upon arrival at the laboratory to preserve their physicochemical integrity. Additionally, the geographic coordinates of each sampling site were recorded using a handheld GPS device with sub-meter accuracy.

Vegetation samples were also collected at each sampling site, including multiple species whenever possible. The sampled taxa included one tree species (*Quercus ilex*), two shrub species (*Retama sphaerocarpa* and *Scrophularia canina*), and three annual herbaceous species (*Hirschfeldia incana, Rumex bucephalophorus*, and *Spergularia rubra*). For the tree species, mature leaves were sampled from multiple individuals per site when available, avoiding both senescent and newly emerged leaves (typically located at the basal and apical portions of branches, respectively). In the case of annual herbs, the entire aerial part of at least ten individuals per species was collected to ensure representativeness. All plant material was stored in paper envelopes to allow for adequate drying and prevent fungal growth, and samples were processed within 10 days of collection to preserve their biochemical integrity.

*Sample preparation*

The preparation of soil samples started with their drying (in opened plastic bag for 15 days). Once dry, they were sieved to discard the > 2 mm fraction, which was weighted to make a rough estimation of their gravel content. The < 2 mm fraction was homogenized and subdivided into three aliquots: one for physicochemical determinations without further treatment, a second aliquot was grinded in an agata mortar to < 100 µm size for chemical analysis, and a third was retained as a backup sample.

Plant samples were washed with tap water followed by deionised water. Afterward, they were dried in a laboratory stove prior to a trituration using a KINEMATICA mixer (MB800 B). A portion of the homogenized samples was separated for Hg analysis, while a second aliquot (5 g) was blended with 0.15 g of agglutinant (dissolution of Elvacite 2046 PANalytical and ACETONA PURISS ($CH_3(CO)CH_3$), UN 1090). The mixture was inserted into aluminium vessels (RETSCH PP25) and compressed using a hydraulic hand press (SPECAC 250 kN) to obtain a pressed pill, utilized in the analytical procedure for X-Ray Fluorescence (XRF) analysis.

Analytical methods

The physicochemical properties of the soils, including reactivity (pH), salts contents based on electric conductivity (EC), and organic matter content, were determined using conventional methods according to the standards UNE-ISO 10390:2012 for pH (AENOR, 2012) and UNE 77308:2001 for EC (AENOR, 2001). In particular, pH and EC measurements were determined after dispersion of the sample in water at a soil/water ratio of 10 gr/50 mL; in the resulting dispersion, the reactivity was estimated using a CRISON GLP 22 pHmeter, and the EC, with a CRISON GLP 32 conductivimeter. The organic matter content (SOM) was estimated using the method proposed by Walkey & Black (1934), based on quantitative oxidative valuation of 1 soil suspension using a mixture of sulphuric acid and K dichromate. The grain size distribution was evaluated using a Fritsch ANALYSETTE MicroTec Plus device, following the procedure outlined by Garcia-Ordiales et al. (2018), and applying the traditional sand-silt-clay classification (Udden-Wentworth, 1922).

Both soil and vegetal samples were analysed for Hg and multielement. Hg analysis was performed by means of atomic absorption spectrometry with Zeeman effect, using a LUMEX RA-915M device (Sholopov et al., 2004). Multielemental analysis was performed via X-ray fluorescence with energy dispersion (EDXRF), using a Malvern Panalytical Epsilon 1 device.

Certified Reference Materials of soils (NIST 2710A) and plants (GC7162) were analysed to ensure precision and accuracy. PTE recovery rates were in the range of 93–114% (XRF) and 94–103% for Hg (ZAAS-HFM).

Soil to plant transfer indices

The bioaccumulation coefficients (BAC) were formulated (Eq. (1) as a simple parameter to assess the bioavailability of elements in the soil, and the capacity of the plant to uptake them (Inacio et al. 2014; Gruszecka-Kosowska 2019).

$$(BAC) = \frac{[C\text{plant}]}{[C\text{soil}]}$$

1

where [$C$plant] and [$C$soil] represent the concentration (in mg $kg^{-1}$) of a given element in the leaves and soil, respectively, corresponding to the same sampling site. Values of BAC > 1 indicate a high bioaccumulation capacity, especially when BACs are calculated with total concentration in soil. The BACs calculated with the soluble fraction in soil are higher, although they more precisely express the hyperaccumulator condition of the plant in a certain polluted substrate.

Statistical Analyses and Mapping

Data treatment involved multivariate analyses performed using Minitab 19.1 and STATGRAPHICS Centurion v19.1.2. Hierarchical clustering was applied to explore relationships among variables, using Ward's linkage method and correlation coefficient distance as the similarity measure. Spatial distribution patterns were generated by inverse distance squared interpolation with Surfer 21.1.158 (Golden Software) and ArcMap 10.8.1 (ArcGIS)."

# RESULTS

Soil analysis

The soil texture shows a prevailing composition of sandy loam soils (average: 75.5% sand, 10.4% silt and 14.1% clay), with higher sand contents located leeward to the sand-sized tailings in agricultural areas. The SOM contents range from 0.1 to 5.8%, with an average of 2.95%, which are common values for soils in this semiarid region (Gallardo, 2016).The lower values (0.1-1%) appear in the soils more clearly affected by the mining activity, intermediate values (1–3%) in soils peripheral to the most affected area, and the highest levels found in agricultural and pasture areas. Soil reactivity is acidic (pH: 5.7 ± 0.7), with the lowest values corresponding to the soils from the proximity of tailings dumps. The contents in salts, as assessed by the EC, show a direct inverse relationship with pH, reaching 12,000 µS $cm^{-1}$ in sites close to mine residua accumulation with the lower pH values. In areas affected less intensely by mining activities, there is no conspicuous relationships among both parameters, with near neutral soil reactivity and EC: 515.9 ± 1,585.4 μS $cm^{-1}$; this high variability in EC is conditioned by the diversity of soil typology in the mine area.

The results of the soil samples are summarized in Table 1. Considering the major elements, it is worth noting that the $SiO_2$ concentrations are relatively constant in terms of the coefficient of variation, although the range of values involved is wide (35.5–71.7%), as observed for $Al_2O3$ and $TiO_2$. This suggests the homogeneity of the geological substrate, primarily constituted by shales and greywackes, but affected by the presence of wine wastes. On the other hand, the maximum variability among major elements is found in CaO, which should be an indication of the occasional presence of carbonates rich in Ca in the mineralized veins. Amongst trace elements, the highest variability corresponds to: Zn > > Pb = Cu > Hg > Sb > S > Ba. This variability is linked to the variability in the abundance of the elements in the deposit and their mobility, which explains a similar variability patterns for Pb and Zn, with Zn being considerably less abundant but exhibiting higher mobility (Rodríguez et al., 2009).

Table 1
Basic statistics for the elemental analysis of the soil samples. Abbreviations: SD: standard deviation; VC: Variation coefficient (in %).

| Variable | Unit | Average | SD | VC | Minimum | Maximum |
|---|---|---|---|---|---|---|
| $SiO_2$ | % | 58.8 | 8.3 | 14.0 | 35.5 | 71.8 |
| $Al_2O_3$ | % | 12.4 | 3.3 | 26.4 | 5.0 | 19.9 |
| CaO | % | 0.8 | 0.9 | 105.3 | 0.1 | 3.9 |
| $Fe_2O_3$ | % | 4.6 | 3.0 | 64.3 | 1.7 | 14.3 |
| $K_2O$ | % | 2.2 | 0.5 | 24.5 | 1.3 | 3.2 |
| $P_2O_5$ | % | 0.2 | 0.1 | 43.5 | 0.1 | 0.5 |
| $TiO_2$ | % | 0.7 | 0.1 | 18.0 | 0.5 | 0.9 |
| S | *mg kg$^{-1}$* | 4,295.0 | 7,328.0 | 170.6 | 304.0 | 25,819.0 |
| Cr | *mg kg$^{-1}$* | 76.5 | 20.1 | 26.3 | 38.4 | 109.6 |
| Mn | *mg kg$^{-1}$* | 868.0 | 733.0 | 84.4 | 124.0 | 3,080.0 |
| Cu | *mg kg$^{-1}$* | 185.1 | 357.0 | 192.9 | 18.1 | 1,680.0 |
| Zn | *mg kg$^{-1}$* | 3,388.0 | 10,004.0 | 295.3 | 68.0 | 48,460.0 |
| Sb | *mg kg$^{-1}$* | 111.9 | 190.4 | 170.2 | 13.1 | 805.6 |
| Hg | *mg kg$^{-1}$* | 232.8 | 427.1 | 183.5 | 3.0 | 1,920.0 |
| Pb | *mg kg$^{-1}$* | 8,000.0 | 15,913.0 | 198.9 | 70.0 | 57,270.0 |
| Rb | *mg kg$^{-1}$* | 72.0 | 22.4 | 31.1 | 42.2 | 121.4 |
| Sr | *mg kg$^{-1}$* | 58.2 | 30.7 | 52.8 | 25.9 | 139.9 |
| Zr | *mg kg$^{-1}$* | 466.3 | 204.2 | 43.8 | 147.8 | 894.0 |
| Sn | *mg kg$^{-1}$* | 69.9 | 17.5 | 25.1 | 53.3 | 123.6 |
| Ba | *mg kg$^{-1}$* | 602.0 | 628.0 | 104.3 | 147.0 | 2,580.0 |

The cluster analysis of soil data results in the dendrogram shown in Fig. 2 for the different elements. Three major clusters (Cl) have been distinguished: Cl1 groups Al, Rb, K and Cr; this appears as a geogenic cluster related to compositional differences in soil composition. Cl2 includes S, Fe, Sb, Sn, Pb Ba, Cu, Zn, and, with minor similarity, Ca and Sr, which includes most of the PTEs characteristic of the mineralogy of the exploited ore deposit. Finally, Cl3 includes Si and Hg with P, Zr, Ti and Mn, what should be related to the presence of cinnabar mineralized rocks, coming from El Entredicho mine in Almadén, to test the froth flotation of this ore; Si is the main component of these samples, since the cinnabar is hosted by quartzites; and P, Zr, Ti and Mn could be also related to the presence, together with the mineralized quartzites, of big boulders of the magmatic rock which, together with the quartzites, host the cinnabar deposit of El Entredicho mine (Hernández et al., 1999).

Besides, the dendrogram from the cluster analysis of samples (Fig. 2) clearly differentiates between three types of samples, which, furthermore, corresponds clearly with three domains with different degrees of contamination (Fig. 3): a highly contaminated domain, coincidental with the central area (brown colour), where the mine wastes, with high marginal contents in ore minerals, persist although substantial dismantling efforts; a second domain, corresponding to tailings from the froth flotation wastes, with intermediate level of contamination (red colour); a third domain corresponding to samples from marginal areas, characterized by limited contamination (green colour).

The PCA analysis, illustrated in Fig. 4, effectively discriminates soil samples according to their geochemical composition and substrate. The first two principal components explain a cumulative 62% of the total variance (47.1% by the first component and 14.9% by the second), providing a robust basis for interpreting the main geochemical gradients. Samples with negative scores on the first component are primarily associated with peripheral soils, characterized by low concentrations of lithogenic elements such as Si, Zr, Ti, and Mn, and relatively higher levels of Zn, Cu, Pb, Sb, Ba, Ca, S, Sn, Fe, and Sr (elements typically linked to anthropogenic inputs). The second component separates samples with elevated concentrations of P, Mn, and Zr (positive scores) from those with higher Hg content (negative scores). Former waste samples are mainly distributed along the positive side of the first component, reflecting their enrichment in ore-related elements, while their position along the second component is more variable, though predominantly negative. In contrast, tailing samples cluster near the origin, with low scores on both components, indicates a more homogeneous and less extreme geochemical profile.

Plant analysis

Table 2 synthetizes the analytical results for the studied plant species. We consider interesting to notice that the concentrations of primary and secondary macronutrients (K, S, and Ca) vary significantly among the species. For instance, *S. rubra* shows very high concentrations of K and S compared to *Q. ilex* and *R. sphaerocarpa*, which present levels roughly an order of magnitude lower. Meanwhile, the concentration of Ca in *H. incana* is about one order of magnitude lower than that found in the rest of the analysed species. These differences can be explained by species-specific physiological traits and ecological adaptations common in Mediterranean ecosystems. Species like *S. rubra* tend to accumulate higher amounts of potassium and sulfur, which are critical for processes such as osmotic regulation and protein synthesis, particularly in plants adapted to nutrient-rich or rapidly growing environments (Kruger, 1983; Sardans & Peñuelas, 2013).

Conversely, the markedly lower Ca concentration in *H. incana* may reflect adaptations to soils with low Ca availability or acidic conditions, a pattern reported in species thriving in nutrient-poor substrates (Groves, 1983; Read & Mitchell, 1983). Overall, these nutrient concentration patterns align with the observed functional traits and phylogenetic differences that influence nutrient cycling and uptake strategies in Mediterranean plant communities (Prieto-Rubio et al., 2022), supporting that such variability is typical and expected in similar ecosystems.

Considering the trace elements, both those considered as micronutrients, common in plants, and toxic for plants, and considering than most of them display a high to extreme variability in the soils of the area, the variability has two conditions: the one considering the different species, and the one considering the different specimens of the same species. The species with higher concentrations in the different elements are: Cu: *S. rubra* ~ *R. bucephalophorus* > all the rest; Fe: *S. rubra* > > *H. incana* ~ *R. bucephalophorus* > *Q. ilex* > *S. canina* > > *R. sphaerocarpa*; Mn: *Q. ilex* > *S. rubra* > *R. bucephalophorus* > *H. incana* > *R. sphaerocarpa* > *S. canina*; Zn: *S. rubra* > *R. bucephalophorus* > > *R. sphaerocarpa* ~ *H. incana* ~ *S. canina* > *Q. ilex*; Hg: S. *rubra* > all the rest; and Pb: *S. rubra* > > *R. bucephalophorus* > > *Q. ilex* > the rest.

Therefore, the plants with higher bioaccumulation capacity, considering the elements related with the mining activity, should be *S. rubra* and *R. bucephalophorus*, with *Q. ilex* also showing a noticeable capacity, in particular for Mn and Pb. Additionally, rubidium (Rb) and strontium (Sr) were analysed due to their chemical similarity to K and Ca, respectively. However, their concentrations were generally low and showed no consistent pattern among species, suggesting limited physiological relevance in this context.

On the other hand, intraspecies variability, as expressed by the variation coefficient, is maxima for Hg in *R. sphaerocarpa* (for very low total concentrations), in *Q. Ilex*, and in *S. rubra* (229.9, 183.2 and 163.8%, respectively); Rb in *S. canina* (141.1%); and Pb in *R. bucephalophorus, Q. ilex* and *R. Sphaerocarpa* (148.4, 123.7 and 120.0% respectively). These variation coefficients are the best indications for a real variability in the bioaccumulation into each species, since these represent the variability related with variations in the contents and therefore, of bioavailability in the soil.

Table 2
Mean, standard deviation, and coefficient of variation for primary and secondary macronutrients, micronutrients, common plant elements, and toxic elements in leaf tissues. All values are expressed in mg $kg^{-1}$, except for Hg, which is expressed in µg $g^{-1}$.

| | *Primary macronutrient* | *Secondary macronutrients* | | *Micronutrients* | | | | *Common elements in plants* | | *Toxic elements for plants* | |
|---|---|---|---|---|---|---|---|---|---|---|---|
| | **K** | **S** | **Ca** | **Cu** | **Fe** | **Mn** | **Zn** | **Sr** | **Rb** | **Hg** | **Pb** |
| **Quercus ilex (n = 23)** | | | | | | | | | | | |
| Mean | 5,286.7 | 1,554.1 | 5,887.7 | 16.0 | 682.0 | 341.5 | 124.5 | 8.1 | 2.5 | 10.4 | 132.9 |
| SD | 1,474.2 | 659.8 | 2,570.7 | 5.2 | 480.9 | 264.7 | 83.4 | 4.2 | 1.5 | 19.0 | 164.3 |
| VC (%) | 27.9 | 42.5 | 43.7 | 32.4 | 70.5 | 77.5 | 67.0 | 51.8 | 58.8 | 183.2 | 123.7 |
| **Retama sphaerocarpa (n = 26)** | | | | | | | | | | | |
| Mean | 7,659.2 | 1,922.3 | 8,437.9 | 19.1 | 225.7 | 86.6 | 274.9 | 17.2 | 4.0 | 4.2 | 36.3 |
| SD | 3,485.5 | 625.9 | 3,173.4 | 6.5 | 83.5 | 38.2 | 202.6 | 12.1 | 2.8 | 9.3 | 43.8 |
| VC (%) | 45.5 | 32.6 | 37.6 | 34.1 | 37.0 | 44.1 | 73.7 | 70.5 | 70.4 | 224.9 | 120.9 |
| **Scrophularia canina (n = 6)** | | | | | | | | | | | |
| Mean | 16,718.0 | 2,695.8 | 8,664.8 | 15.3 | 466.7 | 40.4 | 221.0 | 11.8 | 9.0 | 5.8 | 67.8 |
| SD | 5,362.9 | 364.0 | 1,644.1 | 3.3 | 357.6 | 20.2 | 233.8 | 6.2 | 12.8 | 6.2 | 50.5 |
| VC (%) | 32.1 | 13.5 | 19.0 | 21.7 | 76.6 | 49.9 | 105.8 | 52.8 | 142.1 | 107.2 | 74.4 |
| **Hirschfeldia incana (n = 7)** | | | | | | | | | | | |
| Mean | 21,601.7 | 10,631.4 | 29,098.6 | 11.1 | 966.6 | 104.8 | 222.7 | 91.1 | 11.1 | 10.1 | 54.7 |
| SD | 4,141.1 | 1,797.8 | 12,216.9 | 2.0 | 593.9 | 76.9 | 130.9 | 48.5 | 9.7 | 10.5 | 47.8 |
| VC (%) | 19.2 | 16.9 | 42.0 | 18.3 | 61.4 | 73.4 | 58.8 | 53.2 | 86.6 | 103.5 | 87.4 |
| **Spergularia rubra (n = 8)** | | | | | | | | | | | |
| Mean | 40,414.3 | 5,111.3 | 6,217.1 | 36.1 | 2,711.5 | 290.5 | 1,232.3 | 7.3 | 49.9 | 27.6 | 1,459.6 |
| SD | 9,017.0 | 3,650.5 | 2,524.9 | 21.3 | 2,359.7 | 128.6 | 950.3 | 3.9 | 20.9 | 45.2 | 1,632.4 |
| VC (%) | 22.3 | 71.4 | 40.6 | 58.9 | 87.0 | 44.3 | 77.1 | 53.5 | 42.0 | 163.8 | 111.8 |
| **Rumex bucephalophorus (n = 7)** | | | | | | | | | | | |
| Mean | 24,512.9 | 2,259.3 | 4,848.0 | 22.0 | 960.7 | 154.0 | 927.0 | 8.7 | 8.7 | 8.9 | 552.0 |
| SD | 4,937.4 | 609.8 | 1,969.1 | 6.6 | 545.8 | 119.5 | 455.5 | 3.5 | 6.6 | 9.1 | 819.3 |
| VC (%) | 20.1 | 27.0 | 40.6 | 29.9 | 56.8 | 77.6 | 49.1 | 40.1 | 75.5 | 102.9 | 148.4 |
| Barquero et al. (2024) **(Q. ilex)** | | | | | | | | | | | |
| Mean | 4,000.0 | 1,032.3 | 7,000 | 7.2 | 322.9 | 833.6 | 26.4 | 12.7 | 2.5 | 0.114 | 0.8 |
| **Monaci et al. (2022) (Q. ilex)** | | | | | | | | | | | |
| Mean | 6,000.0 | 1,300.0 | * | 6.1 | 240.0 | * | 34.6 | * | * | 0.06 | 3.1 |
| **Higueras et al. (2016) (Q. ilex)** | | | | | | | | | | | |
| Mean | * | * | * | 4.6 | * | * | 20.6 | * | * | 19.71 | 1.5 |
| Marschner (2012**)** | | | | | | | | | | | |

| | Primary macronutrient | Secondary macronutrients | | Micronutrients | | | | Common elements in plants | | Toxic elements for plants | |
|---|---|---|---|---|---|---|---|---|---|---|---|
| Mean | 10,000.0 | 1,000.0 | 5,000.0 | 6.0 | 100.0 | 50.0 | 20.0 | * | * | * | * |
| **Kabata-Pendias (2001) (Mature leaf tissue generalized for various species)** | | | | | | | | | | | |
| Mean | * | * | * | 5–30 | * | 30–300 | 27–150 | 10–662 | 20–70 | < 1 | 5–10 |
| Toxicity level | * | * | * | 20–100 | * | 400-1,000 | 100–400 | * | * | 1–3 | 30–300 |

The PCA performed on the elemental concentrations in plant tissues (Fig. 5) revealed clear species-specific clustering patterns, reflecting distinct uptake strategies and affinities for PTEs. The first two components accounted for 59.7% of the total variance (PC1: 35.6%, PC2: 24.1%). *Spergularia rubra* exhibited the highest scores along PC1, which was primarily associated with PTEs such as Cu, Zn, Pb, and Hg, as well as Rb, Fe, and K, indicating a strong bioaccumulation capacity. *Hirschfeldia incana* was clearly separated along PC2, showing highly negative values, and positive PC1 scores, suggesting a distinct elemental profile dominated by Mn, Sr, and Ca. *Rumex bucephalophorus* occupied the upper left quadrant, with positive values on both PC1 and PC2, indicating a mixed accumulation pattern. In contrast, *Quercus ilex*, *Retama sphaerocarp*a, and *Scrophularia canina* clustered in the lower left quadrant, with predominantly negative PC1 values and low PC2 scores, reflecting lower accumulation of PTEs and a more conservative elemental uptake strategy. These results underscore the functional diversity among species in response to soil contamination and support the potential use of *S. rubra* and *R. bucephalophorus* as fine bioindicators in metal-impacted environments.

# DISCUSSION

Relationships between concentrations in soil and plant

Elemental concentrations in plants do not necessarily depend on total concentrations in soils. We evaluated this relationship and found that the studied species exhibited contrasting responses in terms of bioaccumulation of secondary macronutrients, common plant elements, and toxic elements, relative to their concentrations in the soil.

Among the studied species, contrasting patterns were observed regarding Ca bioaccumulation in relation to its soil concentration (Fig. 6). *R. bucephalophorus* showed a positive linear correlation (Ca in plant tissue = 0.166 × Ca in soil – 3,571.6; $R^2 = 0.62$), indicating that approximately 62% of the variability in Ca content in plant tissues can be explained by its concentration in the soil. This relationship suggests an efficient Ca uptake strategy in this species, possibly linked to its annual life cycle and opportunistic nutrient acquisition behaviour (White & Broadley, 2003; Marschner, 2012). In contrast, *S. canina* exhibited a moderate negative correlation (Fig. 6, left; $R^2 = 0.60$), where higher soil Ca concentrations were associated with lower tissue concentrations. This may reflect physiological regulation mechanisms to prevent toxicity or ionic imbalances, particularly in acidic soils with high electrical conductivity. Such responses have been reported in plants adapted to nutrient-poor or acidic soils, where tight control of Ca transport becomes essential (Pathak et al., 2021). The limited mobility of Ca in the phloem and its dependence on transpiration flow also influence its redistribution, especially in young tissues or under stress conditions (White & Broadley, 2003). These differences highlight interspecific adaptive strategies to variable edaphic conditions, with *R. bucephalophorus* acting as an efficient accumulator species, while *S. canina* appears to exert stricter control over Ca uptake, likely as a protective response to adverse soil conditions, thereby avoiding associated toxicities and maintaining cellular ionic homeostasis (Wang & Schreiber, 2024).

Figure 7 shows the relationship between Sr concentrations in soil and plant tissues for *S. canina.* The data reveal a moderately negative linear trend, described by the regression equation: $y = -0.485x + 35.9$ ($R^2 = 0.48$), indicating that approximately 48% of the variation in plant Sr content can be explained by its concentration in the soil.

This inverse relationship suggests the presence of a regulatory mechanism in Sr uptake; whereby increased soil availability does not result in a higher accumulation in plant tissues. This behaviour may be attributed to the chemical similarity between Sr and Ca, which can lead to competitive inhibition at the root uptake level, particularly in species adapted to low Ca environments (Gupta & Walther, 2018). Such mechanisms have been documented in various taxa, especially under radiostrontium contamination, where plants exhibit selective exclusion or compartmentalization strategies to mitigate potential toxicity (Chatterjee et al., 2019). Similar responses have also been observed under environmental stress or metal contamination, where selective exclusion mechanisms are activated to maintain ionic homeostasis (Ghori et al., 2019).

Figure 8 shows the relationships between total mercury (THg) concentrations in soils and plant tissues of the different studied species. Based on the observations, it is important to highlight that the San Quintín mining complex is characterized by significant local sources of Hg (e.g., ruins of the former ore-washing facility). In this area, atmospheric Hg ($Hg^0$) has been reported as a relevant component of environmental pollution (Esbrí et al., 2010), supporting the hypothesis that Hg content in plants may reflect atmospheric deposition (Stamenkovic & Gustin, 2009; Barquero et al., 2019; Naharro et al., 2020). In the studied area, the soils emit variable concentrations of $Hg^0$, depending on their proximity to the Hg wastes shown in Fig. 1. Therefore, it is proposed that Hg transfer to plants largely responds to atmospheric contamination originated from the soil compartment (Esbrí et al., 2016; Barquero et al., 2019; Naharro et al., 2019).

In *R. bucephalophorus*, a small-sized plant, a strong exponential relationship is observed (THg plant tissue = 7.888 ln (THg soil) – 32.30; $R^2 = 0.98$). This suggests that proximity to the soil facilitates foliar uptake via air due to exposure to resuspended $Hg^0$ particles in the lower atmospheric layers. This logarithmic accumulation pattern reinforces the potential use of this species as a bioindicator in Hg contaminated environments. Differences in regression slopes among species may be partly explained by their life strategies: annual species (e.g., *R. bucephalophorus*) accumulate Hg over a short vegetative cycle (logarithmic model), whereas biennial or perennial species (e.g., *H. incana* or *S. canina*) are exposed to $Hg^0$ over multiple years, resulting in accumulation patterns better described by linear models. This supports the hypothesis that plant Hg concentrations reflect a spatiotemporal integration of contaminant exposure rather than a direct response to soil content (Kyllmar et al., 2011).

Leaf area is a critical factor influencing the absorption of $Hg^0$. Plants with larger leaf surfaces exhibit a greater capacity for dry deposition and stomatal uptake of elemental $Hg^0$ (Laacouri et al., 2013; Wohlgemuth et al., 2021). Although *Q. ilex* and *R. sphaerocarpa* show low correlations with soil Hg ($R^2$ = 0.07 and 0.12, respectively), this does not preclude significant Hg accumulation. Their large stature facilitates diffuse atmospheric deposition, enhancing $Hg^0$ uptake through stomata and cuticle, particularly during nighttime hours. In the case of *R. sphaerocarpa*, its smaller leaves may limit direct uptake yet still intercept $Hg^0$ previously redistributed in the air. Although specific measurements of Hg in stems are lacking, literature suggests that root-shoot translocation in small plants is possible but rarely complete (e.g., Houttuynia; Greger et al., 2005; Laacouri et al., 2013). Given the known Hg emission sources, the vegetative morphology of each species and their spatial relationship to these sources significantly contribute to explaining the Hg concentrations detected in plant tissues beyond simple a correlation with the soil content.

Bioaccumulation and transfer of elements from soil to plant

The bioaccumulation coefficients (BAC) obtained for the six plant species show notable variability among elements and species, reflecting physiological differences in their capacity to absorb and accumulate nutrients, common elements, and toxic metals. Potassium, a primary macronutrient essential for osmoregulation and enzymatic activation, exhibited the highest values in *S. rubra* (2.05), followed by *H. incana* (1.22), suggesting an efficient adaptation to K deficient soils. Regarding secondary macronutrients, Ca and S showed significant accumulation in *H. incana* (6.12 and 10.69, respectively), possibly due to its belonging to the Brassicaceae family, known for its resilience in environments with elevated concentrations of heavy metals. The micronutrients Cu, Fe, Mn, and Zn, essential for redox and enzymatic processes, were more highly accumulated by *S. rubra* (Mn: 0.80, Zn: 0.66) and *R. sphaerocarpa* (Cu: 0.34, Zn: 0.41), which may be related to differential expression of metal transporters and the production of chelators such as phytochelatins (Alloway, 2013; Juwarkar & Yadav, 2010). The elements Sr and Rb, common but with no clear biological function, usually absorbed due to chemical similarity with Ca and K, were accumulated in higher proportions by *H. incana* (Sr: 2.01) and *S. rubra* (Rb: 0.72), suggesting a low ionic selectivity in these species.

Table 3
Bioaccumulation Coefficient (BAC) for different elements analysed. Values of BAC > 1 shown in bolds.

| | K | S | Ca | Cu | Fe | Mn | Zn | Sr | Rb | Hg | Pb |
|---|---|---|---|---|---|---|---|---|---|---|---|
| **Quercus ilex** | | | | | | | | | | | |
| Mean ± SD | 0.30 ± 0.10 | **1.21** ± 1.06 | **1.68** ± 1.54 | 0.30 ± 0.24 | 0.30 ± 0.20 | 0.50 ± 0.30 | 0.23 ± 0.41 | 0.16 ± 0.10 | 0.04 ± 0.02 | 0.17 ± 0.25 | 0.12 ± 0.18 |
| Range | 0.16–0.53 | 0.05–4.**18** | 0.21–5.**69** | 0.01–0.94 | 0.01–1.**00** | 0.10–1.**30** | 0.00–1.**96** | 0.04–0.37 | 0.01–0.08 | 0.00–0.88 | 0.00–0.62 |
| **Retama sphaerocarpa** | | | | | | | | | | | |
| Mean ± SD | 0.43 ± 0.22 | **1.35** ± 1.36 | **2.42** ± 2.11 | 0.34 ± 0.32 | 0.10 ± 0.01 | 0.20 ± 0.20 | 0.41 ± 0.59 | 0.33 ± 0.23 | 0.06 ± 0.05 | 0.09 ± 0.18 | 0.02 ± 0.04 |
| Range | 0.18–1.**20** | 0.06–5.**13** | 0.29–8.**96** | 0.01–1.**09** | 0.01–0.20 | 0.01–1.**00** | 0.00–2.**34** | 0.05–0.88 | 0.01–0.23 | 0.00–0.67 | 0.00–0.17 |
| **Scrophularia canina** | | | | | | | | | | | |
| Mean ± SD | 0.76 ± 0.19 | **1.49** ± 0.95 | **2.16** ± 2.07 | 0.26 ± 0.17 | 0.20 ± 0.20 | 0.10 ± 0.10 | 0.10 ± 0.04 | 0.26 ± 0.16 | 0.13 ± 0.16 | 0.02 ± 0.01 | 0.04 ± 0.04 |
| Range | 0.49–1.**00** | 0.12–2.**56** | 0.96–6.**32** | 0.04–0.48 | 0.01–0.50 | 0.01–0.30 | 0.04–0.14 | 0.08–0.52 | 0.04–0.45 | 0.01–0.04 | 0.00–0.10 |
| **Hirschfeldia incana** | | | | | | | | | | | |
| Mean ± SD | **1.22** ± 0.48 | **10.69** ± 5.67 | **6.12** ± 4.42 | 0.25 ± 0.09 | 0.50 ± 0.50 | 0.70 ± **1.30** | 0.47 ± 0.36 | **2.01** ± 1.62 | 0.18 ± 0.22 | 0.27 ± 0.30 | 0.08 ± 0.06 |
| Range | 0.75–2.**11** | **4.82–18.51** | **1.06–12.45** | 0.07–0.31 | 0.01–1.**70** | 0.10–3.**50** | 0.14–1.**16** | 0.54–4.**66** | 0.08–0.66 | 0.03–0.67 | 0.00–0.15 |
| **Spergularia rubra** | | | | | | | | | | | |
| Mean ± SD | **2.05** ± 0.88 | **1.69** ± 1.52 | **3.06** ± 2.10 | 0.22 ± 0.20 | 0.70 ± 0.80 | 0.80 ± 0.80 | 0.66 ± 0.55 | 0.17 ± 0.10 | 0.72 ± 0.45 | 0.12 ± 0.08 | 0.15 ± 0.16 |
| Range | **1.26–4**.02 | 0.12–3.**92** | 0.68–7.**00** | 0.04–0.64 | 0.30–2.**50** | 0.10–2.**70** | 0.00–1.**44** | 0.05–0.34 | 0.35–1.**75** | 0.01–0.23 | 0.02–0.54 |
| **Rumex bucephalophorus** | | | | | | | | | | | |
| Mean ± SD | **1.21** ± 0.37 | 0.62 ± 0.76 | **1.32** ± 0.99 | 0.09 ± 0.07 | 0.20 ± 0.20 | 0.50 ± 0.70 | 0.42 ± 0.39 | 0.15 ± 0.08 | 0.10 ± 0.06 | 0.03 ± 0.01 | 0.03 ± 0.02 |
| Range | 0.76–1.**73** | 0.07–2.**14** | 0.30–2.**55** | 0.01–0.22 | 0.01–0.80 | 0.01–2.**00** | 0.02–1.**18** | 0.07–0.27 | 0.03–0.18 | 0.01–0.05 | 0.01–0.08 |

Regarding toxic elements, Hg and Pb, with lack biological function and highly toxic, generally showed low values, although *H. incana* and *S. rubra* presented relatively elevated Hg levels (0.27 and 0.12, respectively). This is not due to a deficiency in exclusion mechanisms but rather to the direct uptake of elemental $Hg^0$, favoured by the low stature of these species and their proximity to the local soil, acting as a source of Hg emissions. Accumulation of Pb was more homogeneous, with *S. rubra* standing out slightly (0.15). These results suggest that *H. incana* and *S. rubra* possess a broad accumulation profile, including macronutrients, micronutrients, and toxic elements, positioning them as potential candidates for phytoremediation strategies in contaminated soils (Nnaji et al., 2023). The ability of these species to accumulate multiple elements may be related to the expression of nonspecific transporters and the production of chelating compounds such as phytochelatins and metallothioneins, mechanisms widely documented in hyperaccumulator species (Alloway, 2013; Juwarkar & Yadav, 2010).

The interspecific variability observed in BAC reflects evolutionary adaptations to specific environmental conditions, such as nutrient poor or heavy metal contaminated soils, as documented in plant families like Brassicaceae and Scrophulariaceae (Juwarkar & Yadav, 2010; Alloway, 2013). In the case of *Q. ilex*, a perennial woody species characteristic of Mediterranean ecosystems, a moderately low bioaccumulation pattern was observed compared to the herbaceous species analysed here. BAC values were below 1 for most elements, except for Ca (1.68) and S (1.21), indicating a limited accumulation capacity from the soil. This behaviour may be related to its deep root system and conservative nutrient strategy, typical of sclerophyllous species adapted to oligotrophic environments. Although *Q. ilex* has been described by many authors as a Mn bioaccumulator in its tissues (Rodà et al., 1999; Arena et al., 2014; Barquero et al., 2024), in this study it exhibited a relatively low BAC value (0.50). This may be attributed to the limited availability of Mn in acidic soils contaminated with iron. Under these conditions, $Mn^{2+}$ is easily oxidized to insoluble forms such as $MnO_2$, especially in the presence of Fe oxides, reducing its mobility and bioavailability to plants (Paterson et al., 1985; Robson, 1988; Grangeon et al., 2020). As shown in section 3.3, the low height of herbaceous species near the ground may favour the uptake of $Hg^0$, while *Q. ilex*, being a tall species, has less direct exposure to these emissions, capturing only the diffuse concentrations present in the local atmosphere. Altogether, these factors reinforce the role of *Q. ilex* as a resilient species with efficient regulatory mechanisms for element uptake, even in heavily anthropized environments, as demonstrated by Barquero et al, (2024).

# CONCLUSIONS

The findings of this study confirm that the San Quintín abandoned mining area constitutes a highly contaminated environment, with elevated concentrations of PTEs in soils and mining residues. The detailed geochemical characterization revealed significant spatial heterogeneity in PTE distribution and speciation, reflecting the legacy of diverse mining activities and waste management practices over more than a century.

The analysis of plant–soil interactions demonstrated marked inter- and intraspecific variability in the uptake and bioaccumulation of elements such as Zn, Pb, Hg, and Cu. Notably, *Spergularia rubra* and *Rumex bucephalophorus* exhibited high accumulation capacities, underscoring their potential as effective bioindicators and possible candidates for phytoremediation in metal-contaminated environments. These patterns were closely linked to both edaphic factors and species-specific physiological traits, highlighting the complexity of PTE transfer mechanisms.

A particularly relevant outcome of this study is the assessment of atmospheric deposition as a key pathway for mercury accumulation in plant tissues. The results indicate that Hg uptake is not solely governed by soil concentrations, but also by proximity to Hg discrete emission sources, plant stature, and leaf surface area—factors that modulate exposure to gaseous elemental mercury ($Hg^0$) in the local atmosphere.

Overall, this work advances our understanding of the multifactorial processes governing PTEs dynamics in degraded ecosystems. It provides a scientific basis for the development of ecological restoration strategies and environmental monitoring frameworks in decommissioned mining areas, with broader implications for risk assessment and land management in similarly affected regions.

# References

1. Adamo, P., Lavazzo, P., Albanese, S., Agrelli, D., De Vivo, B., & Lima, A. (2014). Bioavailability and soil-to-plant transfer factors as indicators of potentially toxic element contamination in agricultural soils. Science of the Total Environment, 500, 11–22. https://doi.org/10.1016/j.scitotenv.2014.08.085
2. AENOR (2001). UNE 77308:2001: Calidad del suelo. Determinación de la conductividad eléctrica específica. https://tienda.aenor.com/norma-une-77308-2001-n0024111. (last access June 2024).
3. AENOR (2012). UNE-ISO 10390:2012: Calidad del suelo. Determinación del pH. https://tienda.aenor.com/norma-astm-d4972-01-2007-056326,. (last access June 2024).
4. Alloway, B.J. (2009). Soil factors associated with zinc deficiency in crops and humans. Environmental Geochemistry and Health, 31(5), 537–548. https://doi.org/10.1007/s10653-009-9255-4

5. Alloway, B.J. (2013). Heavy Metals in Soils: Trace Metals and Metalloids in Soils and their Bioavailability (3rd ed.). Springer. https://doi.org/10.1007/978-94-007-4470-7
6. Arena, C., De Maio, A., De Nicola, F., Santorufo, L., Vitale, L., & Maisto, G. (2014). Assessment of eco-physiological performance of Quercus ilex L. leaves in urban area by an integrated approach. Water, Air, & Soil Pollution, 225(1824). https://doi.org/10.1007/s11270-013-1824-6
7. Barquero, J.I., Rojas, S., Esbrí, J.M., García-Noguero, E.M., & Higueras, P. (2019). Factors influencing mercury uptake by leaves of stone pine (*Pinus pinea* L.) in Almadén (Central Spain). *Environmental Science and Pollution Research, 26*(4), 3129–3137. https://doi.org/10.1007/s11356-017-0446-8
8. Barquero, J.I., Lorenzo, S., Rivera, S. et al. Biogeochemical prospecting of metallic critical raw materials: soil to plant transfer in SW Ciudad Real Province, Spain. Environ Sci Pollut Res 31, 29536–29548 (2024). https://doi.org/10.1007/s11356-024-33097-0
9. Chatterjee, S., Mitra, A., Walther, C., & Gupta, D.K. (2019). Plant response under strontium and phytoremediation. En D. K. Gupta & C. Walther (Eds.), Strontium contamination in the environment (pp. 85–97). Springer. https://doi.org/10.1007/978-3-030-15314-4_5
10. Esbrí, J. M., Martín-Crespo, T., Gómez-Ortiz, D., Monescillo, C. I., Lorenzo, S., & Higueras, P. (2010, May). Mercury dispersion in soils of an abandoned lead-zinc-silver mine, San Quintín (Spain). EGU General Assembly 2010, Abstract EGU2010-14998. European Geosciences Union. https://ui.adsabs.harvard.edu/abs/2010EGUGA..1214998E
11. Esbrí, J.M., Martínez-Coronado, A., & Higueras, P. (2016). Temporal variations in gaseous elemental mercury at a contaminated site: Main factors affecting nocturnal maxima in daily cycles. *Atmospheric Environment, 125*, 8–14. https://doi.org/10.1016/j.atmosenv.2015.11.012
12. Ferri-Moreno, I., Barquero-Peralbo, J.I., Andreu-Sánchez, O., García-Lorenzo, M.L., & Esbrí, J.M. (2023). Categorization of mining materials for restoration projects by means of pollution indices and bioassays. Minerals, 13(4), 492. https://doi.org/10.3390/min13040492
13. Galán. E., Romero. A. (2008). Contaminación de suelos por metales pesados. Macla 10, 48-60. ISSN: 1885-7264.
14. Gallardo, J.F. (Ed.). (2016). *The Soils of Spain*. Springer. https://doi.org/10.1007/978-3-319-20541-0
15. Gallego, S., Esbrí, J.M., Campos, J.A., Peco, J.D., Martin-Laurent, F., & Higueras, P. (2021). Microbial diversity and activity assessment in a 100-year-old lead mine. Journal of Hazardous Materials, 410, 124618. https://doi.org/10.1016/j.jhazmat.2020.124618
16. García-Lorenzo, M.L., Crespo-Feo, E., Esbrí, J.M., Crespo, I., & Sánchez-Donoso, R. (2019). Assessment of potentially toxic elements in technosols by tailings derived from Pb–Zn–Ag mining activities at San Quintín (Ciudad Real, Spain): Some insights into the importance of integral studies to evaluate metal contamination pollution hazards. Minerals, 9(6), 346. https://doi.org/10.3390/min9060346
17. García-Ordiales, E., Covelli, S., Rico, J. M., Roqueñí, N., Fontolan, G., Flor-Blanco, G., Cienfuegos, P., & Loredo, J. (2018). Occurrence and speciation of arsenic and mercury in estuarine sediments affected by mining activities (Asturias, northern Spain). Chemosphere, 198, 281–289. https://doi.org/10.1016/j.chemosphere.2018.01.146
18. Ghori, N.H., Ghori, T., Hayat, M.Q., Imadi, S.R., Gul, A., Altay, V., & Ozturk, M. (2019). Heavy metal stress and responses in plants. International Journal of Environmental Science and Technology, 16(3), 1807–1828. https://doi.org/10.1007/s13762-019-02215-8
19. Grangeon, S., Bataillard, P., & Coussy, S. (2020). The nature of manganese oxides in soils and their role as scavengers of trace elements: Implication for soil remediation. In Environmental Soil Remediation and Rehabilitation (pp. 399–429). Springer. https://doi.org/10.1007/978-3-030-40348-5_7
20. Greger, M., Löfstedt, C., & Öborn, I. (2005). Mercury uptake, translocation and accumulation in plants. Environmental Pollution, 138(1), 109–117. https://doi.org/10.1016/j.envpol.2005.02.016
21. Groves, R.H. (1983). Nutrient cycling in Australian heath and South African fynbos. In F. J. Kruger, D. T. Mitchell, & J. U. M. Jarvis (Eds.), Mediterranean-Type Ecosystems: The Role of Nutrients (pp. 179–191). Springer. https://doi.org/10.1007/978-3-642-70868-8_22

22. Gruszecka-Kosowska, A. (2019). Human health risk assessment and potentially harmful element contents in the fruits cultivated in Southern Poland. International Journal of Environmental Research and Public Health, 16(24), 5096. https://doi.org/10.3390/ijerph16245096
23. Gupta, D.K., & Walther, C. (Eds.). (2018). Behaviour of Strontium in Plants and the Environment. Springer International Publishing. https://doi.org/10.1007/978-3-319-66574-0
24. Harries. J.R., Ritchie. A.I.M. (1987) The effect of rehabilitation on the rate of oxidation of pyrite in a mine waste rock dump. Environ. Geochem. Health 9, 27–36 https://doi.org/10.1007/BF01686172
25. Hernández, A., Jébrak, M., Higueras, P., Oyarzun, R., Morata, D., Munhá, J. (1999). The Almadén mercury mining district, Spain. Mineralium Deposita, 34: 539-548. https://doi.org/10.1007/s001260050219
26. Higueras, P., Esbrí, J.M., García-Ordiales, E., Alonso-Azcárate, J., & Martínez-Coronado, A. (2017). Potentially harmful elements in soils and holm-oak trees (Quercus ilex L.) growing in mining sites at the Valle de Alcudia Pb–Zn district (Spain) – Some clues on plant metal uptake. Journal of Geochemical Exploration, 182, 166–179. https://doi.org/10.1016/j.gexplo.2016.10.021
27. Higueras, P., Oyarzun, R., Iraizoz, J.M., Lorenzo, S., Esbrí, J.M., & Martínez-Coronado, A. (2011). Low-cost geochemical surveys for environmental studies in developing a field portable XRF instrument under quasi-realistic conditions. Journal of Geochemical Exploration, 113, 3–12. https://doi.org/10.1016/j.gexplo.2011.02.005
28. Inácio, M., Neves, O., Pereira, V., & da Silva, E. F. (2014). Levels of selected potential harmful elements (PHEs) in soils and vegetables used in diet of the population living in the surroundings of the Estarreja Chemical Complex (Portugal). Applied Geochemistry, 44, 38–44. https://doi.org/10.1016/j.apgeochem.2013.07.017
29. Juwarkar, A.A., & Yadav, S.K. (2010). Bioaccumulation and biotransformation of heavy metals. In M.H. Fulekar (Ed.), Bioremediation Technology: Recent Advances (pp. 265–292). Springer. https://doi.org/10.1007/978-90-481-3678-0_9
30. Kabata-Pendias. A. (2011). Trace elements in soils and plants. Fourth Edition. CRC press LLC. Boca Raton, 331 pp. ISBN: 1420093681
31. Kirkby. E. (2012) Introduction. Definition and Classification of Nutrients. In: Marschner. P. (Ed.). Mineral Nutrition of Higher Plants (Third ed.). pp. 3-5. Academic Press. ISBN: 9780123849052. https://doi.org/10.1016/B978-0-12-384905-2.00001-7
32. Kisku, G.C., Barman, S.C., Bhargava, S.K. (2000). Contamination of soil and plants with potentially toxic elements irrigated with mixed industrial effluent and its impact on the environment. Water Air and Soil Pollution, 120(1-2), pp. 121–137 https://doi.org/10.1023/A:1005202304584
33. Kruger, F. J. (1983). Responses of plants to nutrient supply in Mediterranean-type ecosystems. In F. J. Kruger, D. T. Mitchell, & J. U. M. Jarvis (Eds.), Mediterranean-Type Ecosystems: The Role of Nutrients (pp. 415–427). Springer. https://doi.org/10.1007/978-3-642-70868-8_26
34. Kyllmar, K., Carlsson, C., Gustafsson, D., & Ulén, B. (2011). Temporal dynamics of mercury in crop biomass and implications for long-term trends in agriculture. *Environmental Pollution, 159*(6), 1607–1612. https://doi.org/10.1016/j.envpol.2011.02.016
35. Laacouri, A., Nater, E.A., & Kolka, R.K. (2013). Distribution and uptake dynamics of mercury in leaves of common deciduous tree species in the USA. Environmental Science & Technology, 47(19), 10462–10470. https://doi.org/10.1021/es401357z
36. Marschner, P. (2012). *Marschner's Mineral Nutrition of Higher Plants* (3rd ed.). Academic Press.
37. Molina. J.A., Oyarzun. R., Esbrí. J.M., Higueras. P. (2006). Mercury accumulation in soils and plants in the Almadén mining district. Spain: One of the most contaminated sites on earth. Environmental Geochemistry and Health 28(5), 487-498. https://doi.org/10.1007/s10653-006-9058-9
38. Naharro, R., Esbrí, J.M., Amorós, J.Á., García-Navarro, F.J., & Higueras, P. (2019). Assessment of mercury uptake routes at the soil–plant–atmosphere interface. *Geochemistry: Exploration, Environment, Analysis, 19*(2), 146–154. https://doi.org/10.1144/geochem2018-019
39. Newman, M.C., & Jagoe, C.H. (1994). Inorganic toxicants—Ligands and the bioavailability of metals in aquatic environments. In J.L. Hamelink, P.F. Landrum, H.L. Bergman, & W.H. Benson (Eds.). Bioavailability: Physical, chemical, and biological interactions (pp. 39–61). CRC Press.

40. Nnaji, N. D., Onyeaka, H., Miri, T., & Ugwa, C. (2023). Bioaccumulation for heavy metal removal: A review. *SN Applied Sciences, 5*(125). https://doi.org/10.1007/s42452-023-05351-6
41. Palero. F.J. (1991). Evolución geotectónica y yacimientos minerales de la región del Valle de Alcudia (sector meridional de la Zona Centro Ibérica). Tesis Doctoral. Universidad de Salamanca. 827 pp.
42. Palero, F.J., Both, R., Arribas, A., Mangas, J., & Martín-Izard, A. (2003). Geology and metallogenic evolution of the polymetallic deposits of the Alcudia Valley mineral field, Eastern Sierra Morena, Spain. Economic Geology, 98(3), 577–605. https://doi.org/10.2113/gsecongeo.98.3.577
43. Paterson, E., Goodman, B.A., & Farmer, V.C. (1985). The chemistry of aluminium, iron and manganese oxides in acid soils. In Soil Acidity (pp. 97–124). Springer. https://doi.org/10.1007/978-3-642-74442-6_5
44. Pathak, R.K., Singh, D.B., Sharma, H., & Pandey, D. (2021). Calcium uptake and translocation in plants. En *Calcium Transport Elements in Plants* (pp. 373–386). Elsevier. https://doi.org/10.1016/B978-0-12-821792-4.00018-7
45. Peco, J.D., Higueras, P., Campos, J.A., Esbrí, J.M., Moreno, M.M., Battaglia-Brunet, F., & Sandalio, L.M. (2021). Abandoned mine lands reclamation by plant remediation technologies. Sustainability, 13(12), 6555. https://doi.org/10.3390/su13126555
46. Peco, J.D., Thouin, H., Esbrí, J.M., Campos-Rodríguez, H.R., García-Noguero, E.M., Breeze, D., Villena, J., Gloaguen, E., Higueras, P.L., & Battaglia-Brunet, F. (2023). Mobility of antimony in contrasting surface environments of a mine site: Influence of redox conditions and microbial communities. Environmental Science and Pollution Research, 30(48), 105808–105828. https://doi.org/10.1007/s11356-023-29734-9
47. Prieto-Rubio, J., Perea, A., Garrido, J.L., Alcántara, J.M., Azcón-Aguilar, C., López-García, A., & Rincón, A. (2022). Plant traits and phylogeny predict soil carbon and nutrient cycling in Mediterranean mixed forests. Ecosystems, 25(3), 707–722. https://doi.org/10.1007/s10021-022-00815-z
48. Read, D.J., & Mitchell, D.T. (1983). Decomposition and mineralization processes in Mediterranean-type ecosystems and in heathlands of similar structure. In F. J. Kruger, D.T. Mitchell, & J.U.M. Jarvis (Eds.), Mediterranean-Type Ecosystems: The Role of Nutrients (pp. 208–232). Springer. https://doi.org/10.1007/978-3-642-70868-8_23
49. Robson, A.D. (1988). Manganese in soils and plants—An overview. In R. D. Graham, R. J. Hannam, & N. C. Uren (Eds.), Manganese in Soils and Plants (pp. 329–333). Springer. https://doi.org/10.1007/978-94-009-2817-6_22
50. Rodà, F., Retana, J., Gracia, C.A., & Bellot, J. (Eds.). (1999). Quercus ilex L. ecosystems: function, dynamics and management. Springer. https://doi.org/10.1007/978-94-017-2836-2
51. Rodríguez, L., Ruiz, E., Alonso-Azcárate, J., & Rincón, J. (2009). Heavy metal distribution and chemical speciation in tailings and soils around a Pb-Zn mine in Spain. Journal of Environmental Management, 90(2), 1106–1116. https://doi.org/10.1016/j.jenvman.2008.04.007
52. Sánchez-Donoso, R., Martín-Duque, J.F., Crespo, E., & Higueras, P. (2019). Tailing's geomorphology of the San Quintín mining site (Spain): Landform catalogue, aeolian erosion and environmental implications. Environmental Earth Sciences, 78(5), 166. https://doi.org/10.1007/s12665-019-8148-9
53. Sardans, J., & Peñuelas, J. (2013). Plant-soil interactions in Mediterranean forest and shrublands: Impacts of climatic change. Biogeochemistry, 113(1-3), 1–19. https://doi.org/10.1007/s10533-012-9792-2
54. Sholupov, S., Pogarev, S., Ryzhov, V., Mashyanov, N., & Stroganov, A. (2004). Zeeman atomic absorption spectrometer RA-915+ for direct determination of mercury in air and complex matrix samples. Fuel Processing Technology, 85(6–7), 473–485. https://doi.org/10.1016/j.fuproc.2003.11.003
55. Stamenkovic, J., Gustin, M.S. 2009 Nonstomatal versus stomatal uptake of atmospheric mercury. Environmental Science and Technology 43(5), pp. 1367-1372. https://doi.org/10.1021/es801583a
56. Thalassinos, G., Petropoulos, S. A., Grammenou, A., & Antoniadis, V. (2023). Potentially toxic elements: A review on their soil behavior and plant attenuation mechanisms against their toxicity. Agriculture, 13(9), 1684. https://doi.org/10.3390/agriculture13091684
57. Udden-Wentworth, C.K. A scale of grade and class terms of clastic sediments. J. Geol. 1922, 30, 377–392.

58. Walkley. A. and Black. I.A. (1934) An Examination of the Degtjareff Method for Determining Soil Organic Matter and a Proposed Modification of the Chromic Acid Titration Method. Soil Science 37, 29-38. http://dx.doi.org/10.1097/00010694-193401000-00003
59. Wang, Y., & Schreiber, S.L. (2024). Mechanisms of calcium homeostasis orchestrate plant growth and immunity. *Nature*, 619, 120–130. https://doi.org/10.1038/s41586-024-07100-0
60. White, P.J., & Broadley, M.R. (2003). Calcium in plants. *Annals of Botany*, 92(4), 487–511. https://doi.org/10.1093/aob/mcg164
61. Wohlgemuth, D., Bahlmann, E., & Kesselmeier, J. (2021). Mercury uptake by leaves: A comparison of different plant species and morphologies. Biogeosciences, 18, 6313–6328. https://doi.org/10.5194/bg-18-6313-2021

## Figures

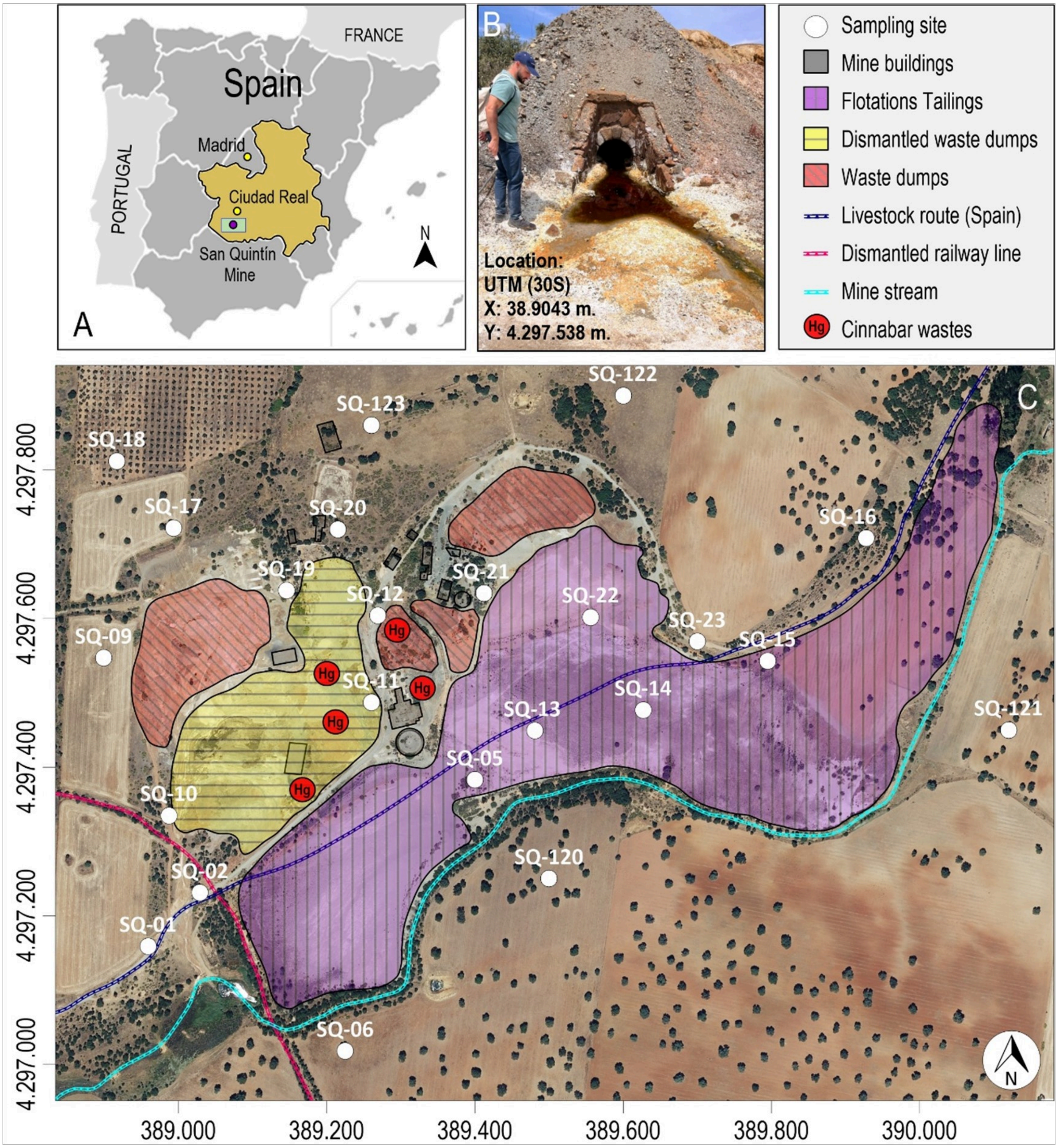


**Figure 1**

(A) Location of the study area in the San Quintín mining district (Ciudad Real, Spain). (B) Mine gallery drainage outlet showing acid mine drainage (AMD) discharge. (C) Detailed site map displaying sampling locations, mining infrastructure, waste deposits (including flotation tailings, olive mill residues, and cinnabar-rich dumps), along with important environmental characteristics relevant to the study.

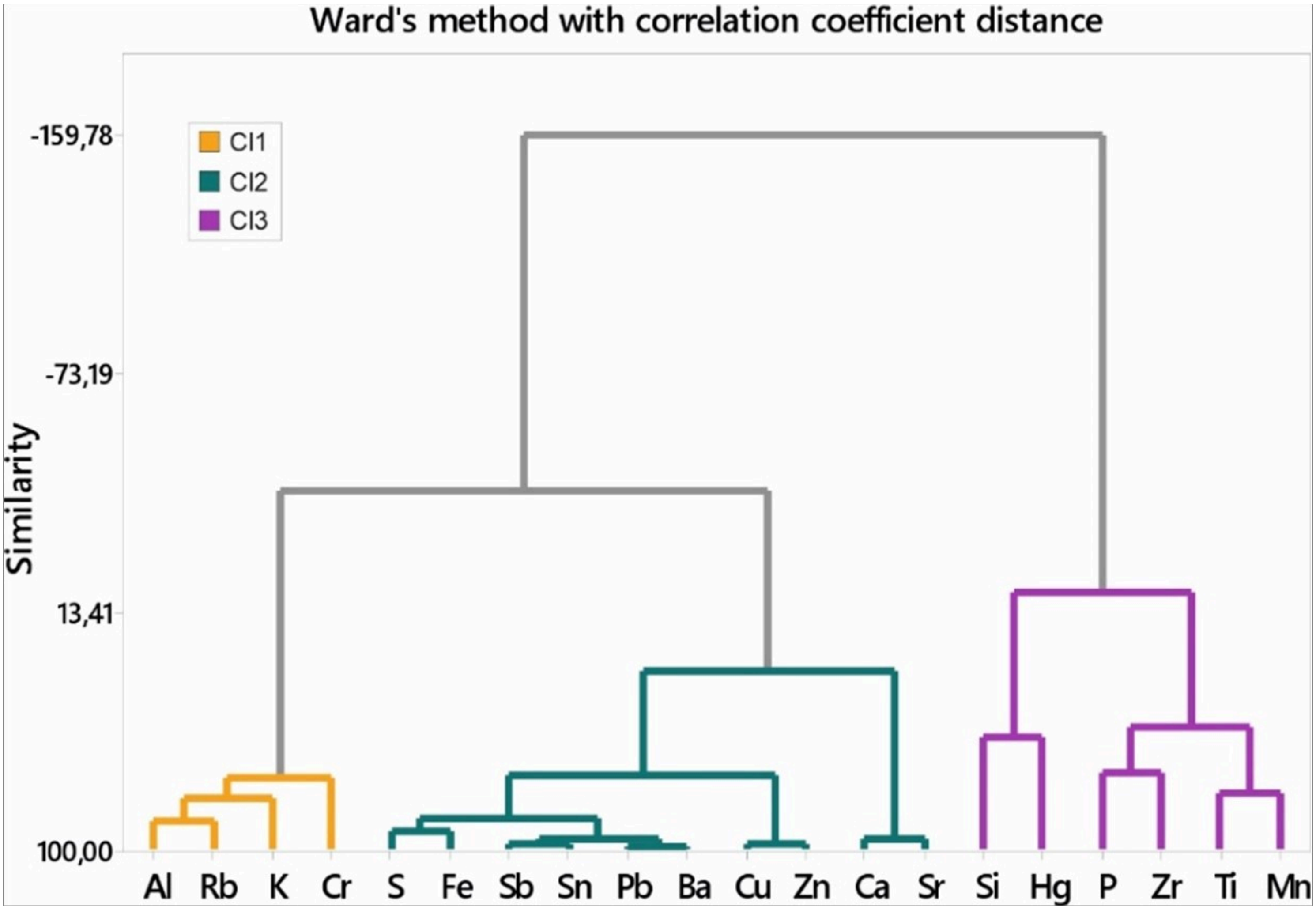


**Figure 2**

Dendrogram for the analytical values for soils.


Figure 3

Scheme showing the location of the samples on the different substrates, as well as the dendrogram confirming the geochemical similarities between the samples taken on these substrates.

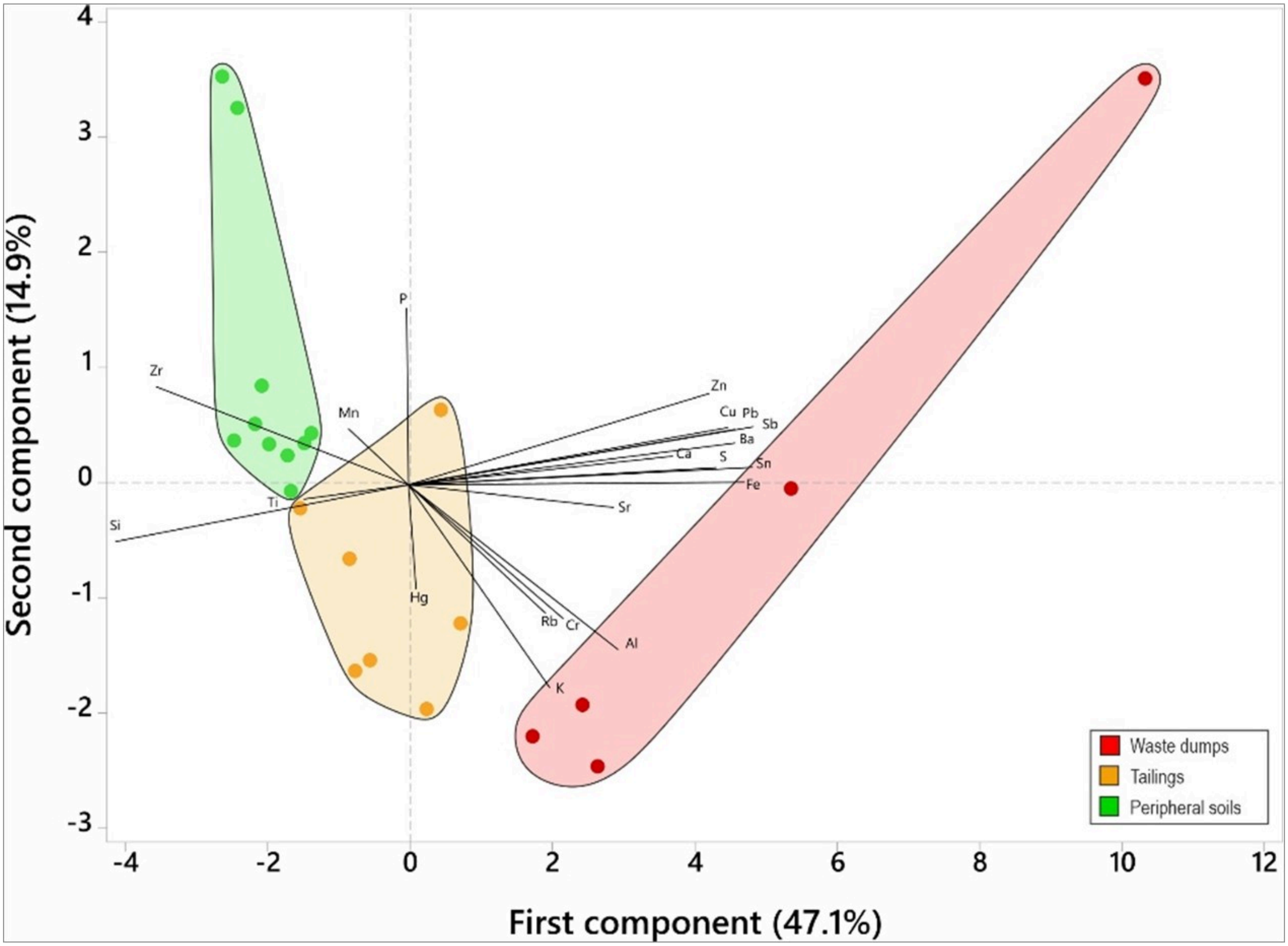


Figure 4

Factor analysis double projection graphic for the two first factors, soil samples grouped by substrate.

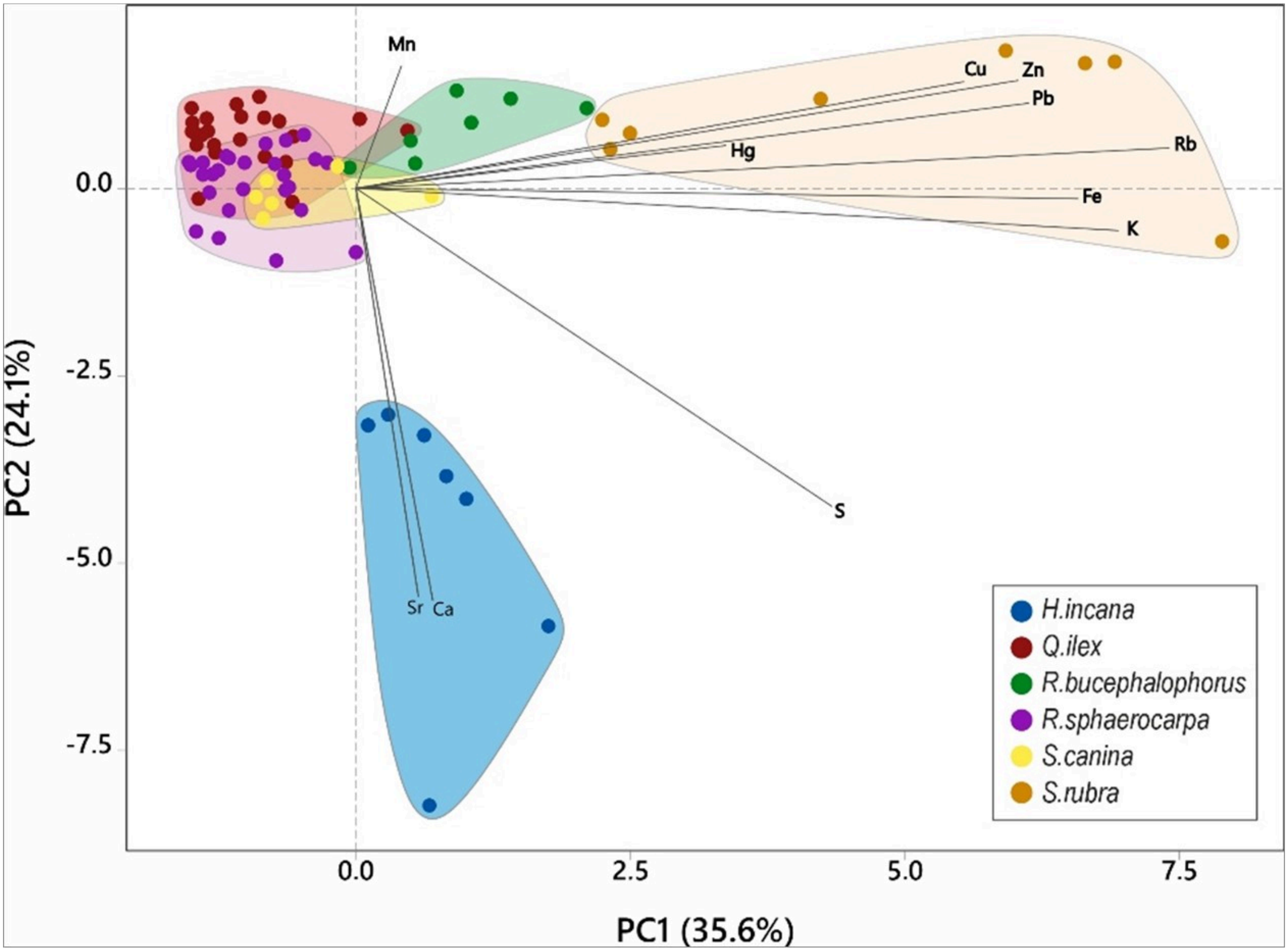


**Figure 5**

Factor analysis double projection graphic for the two first factors, plant samples grouped by species.

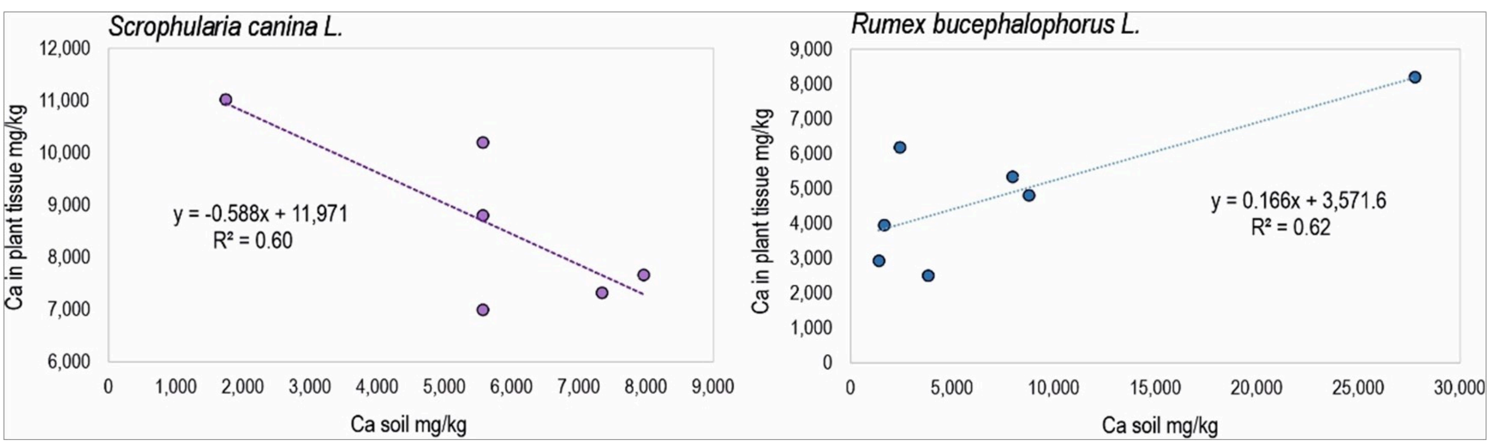


**Figure 6**

Relationship between soil and plant tissue Ca concentrations in two studied species: Scrophularia canina (left), and Rumex bucephalophorus (right).

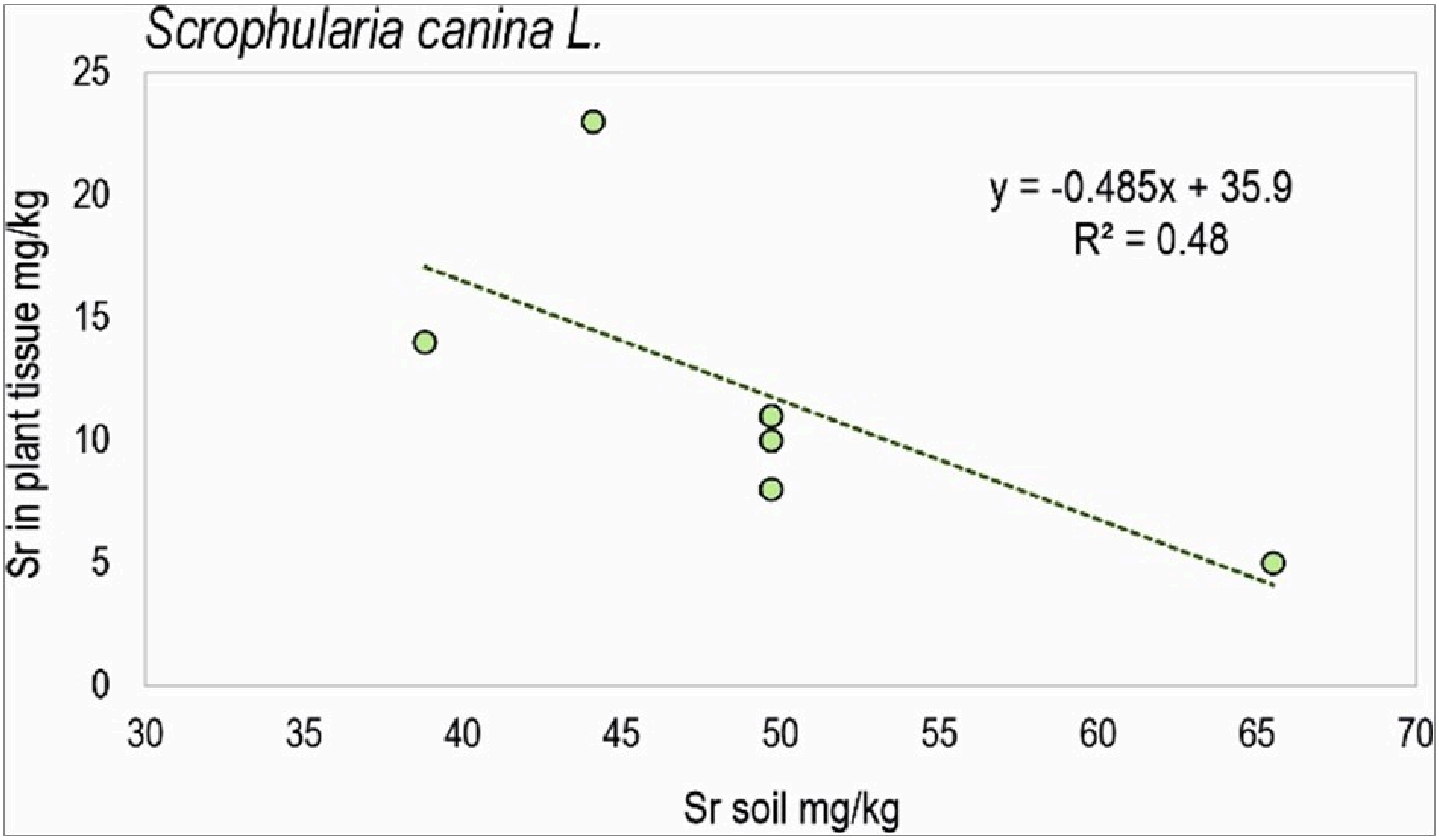


**Figure 7**

*Relationship between soil and plant tissue Sr concentrations in Scrophularia canina.*

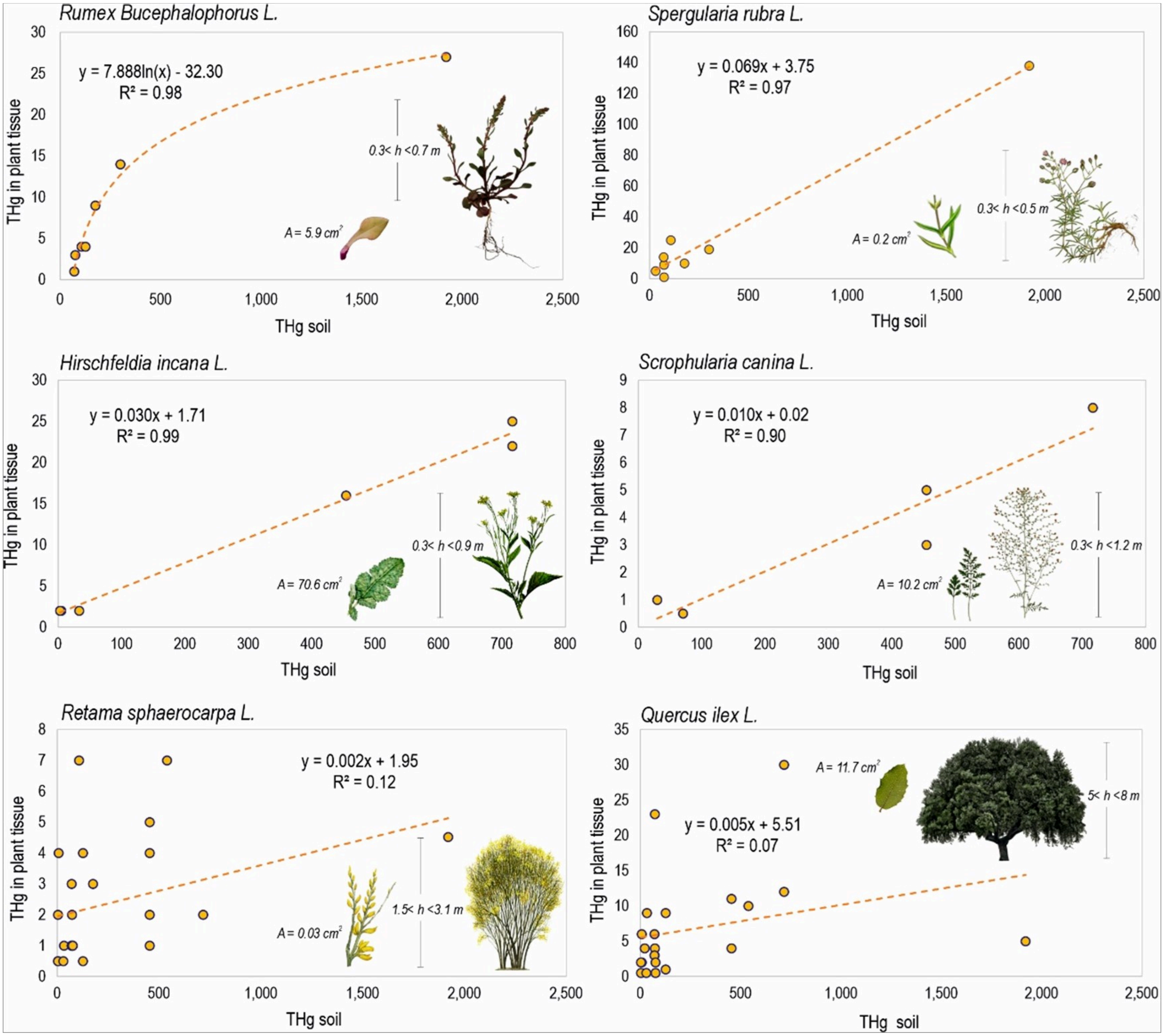


## Figure 8

Relationship between THg concentrations in soil and plant tissues of six species present in the study area, including height range and leaf area of each species.